Morphological study of hydroxyapatite nanocrystal suspension

E. BOUYER*, F. GITZHOFER, M. I. BOULOS
Plasma Technology Research Center (CRTP), Department of Chemical Engineering, Applied Science Faculty, Université de Sherbrooke, Sherbrooke, (Québec) Canada, J1K 2R1
E-mail: etienne.bouyer@dlr.de

Nanometer size hydroxyapatite (HA) crystals are prepared by a wet chemical precipitation method at different synthesis temperatures and with various reactant addition rates. The resulting aqueous suspensions are studied in terms of morphology (transmission electron microscope, specific surface area), phase (X-ray diffraction, electron diffraction and infrared spectroscopy) and rheological properties. This work shows that shape, size and specific surface area of the HA nanoparticles are very sensitive to the reaction temperature and also to the reactant addition rate. The measured pH at the end of synthesis, which is strongly linked with the reactant addition rate, is a key parameter which can be used to determine the purity of the synthesized HA nanocrystal and also for the stabilization (dispersion) of the suspension. HA nanoparticles synthesized at low temperature ($T < 60\,^{\circ}C$) are monocrystalline. A transition temperature ($T = 60\,^{\circ}C$) can be defined as a limit for the synthesis of monocrystalline HA nanocrystals, above this critical temperature nanocrystals become polycrystalline. HA monocrystals adopt a needle shape and are oriented following the *c*-axis of the hexagonal HA structure. The as-synthesized suspension is then concentrated and the effect of a dispersing agent addition, which is needed to get a high solid/liquid ratio coupled with good flowability of the suspension, is also shown, because this suspension is used in the suspension plasma spraying process.

1. Introduction

Hydroxyapatite (HA) is a well known bioceramic dedicated for biomedical applications. HA is currently used for various biomedical applications, such as a bone substitute [1]. HA, which is chemically similar to human hard tissue inorganic matter, can bond to bone without bone resorption when used as a coating on titanium implants [2]. The present study was undertaken to explore the synthesis of a suspension containing HA nanocrystals. A lot of contributions can be found in this field especially concerning the study of the temperature synthesis effect on the resulting nanocrystal morphology [3–5]. This suspension can be used either as a raw material for deposition processing such as sol gel deposition [6] or suspension plasma spraying [7], or for powder processing by atomization or spray drying.

For these kinds of application, HA suspension physico-chemical characteristics are very important because the final material quality (composition, purity, flowability) will be strongly dependent on those characteristics. Obviously, HA is used as a raw material for different shaping processes. One of the key parameters is to control the composition of HA in order to prepare pure HA suspensions. The suspension synthesized is an aqueous colloidal suspension also called sol or gel or physical gel [8, 9].

The objective of this work is to study the effect of different synthesis parameters (reaction temperature, reactant addition rate) on the morphology, phase and rheological properties of the colloidal HA suspension.

2. Materials and methods

HA suspension was prepared by a wet chemical reaction of precipitation following the reaction of Tagai and Aoki [10]:

$$10Ca(OH)_2 + 6H_3PO_4 \rightarrow Ca_{10}(PO_4)_6(OH)_2 + 18H_2O \quad (1)$$

The pH was monitored during the precipitation reaction. The acid is added to calcium hydroxide solution at different speeds. The reactant concentrations are 0.5 mole/1 and 0.3 mole/1 for the calcium hydroxide and for the orthophosphoric acid respectively. The resultant concentration of the suspension is 0.05 mole/1 of HA nanocrystals. Chemical reaction is achieved in a double-wall beaker and heated by the water circulation

*Current address: German Aerospace Center (DLR), Institute for Technical Thermodynamics, Vaihingen, Pfaffenwaldring 38–40, D-70569 Stuttgart, Germany.

from a constant temperature bath. Reaction temperature was varied between 25 to 85 °C. Reaction stirring is performed by a magnetic stirrer. The resulting aqueous suspension is whitish and possesses a solid (HA nanocrystals) content of 2.5 wt %. In order to be used for the suspension plasma spraying process [7], the suspension has to undergo centrifugation and an evaporation process for the elimination of the water leading to a maximum weight ratio solid/liquid to about 40%. In the same way, the suspension viscosity has to be adjusted to a maximum of 10 Pa.s to allow good atomization of the suspension. The first step of the aging process is the natural settling which permits a solid/liquid ratio of 5 wt %. The further centrifugation step allows a value of more than 12 wt % for the same ratio. The final step is to remove water by heating the suspension (under stirring) at a temperature around 80 °C, then the solid/liquid ratio can reach more than 35 wt %.

The flowability of the suspension is optimized with the help of a deflocculant (dispersing agent) which improves the dispersion of the solid particles contained in the suspension by a modification of their surface charge. The dispersing agent employed (Darvan 7, R.T. Vanderbilt Company Inc., Norwalk, CT, USA) is based on sodium polymetacrylate (MW = 16 000) in aqueous solution. Darvan 7 can be used for biomedical applications, because it meets the FDA recommendations in terms of biocompatibility.

The morphology study performed on the HA nanocrystals was done on a transmission electron microscope (TEM, JEOL 100S) apparatus, the specific surface area was measured following the Brunauer-Emmett-Teller (BET) method (Micromeritics Flowsorb II 2300). Concerning the phase study the characterization was performed with both X-ray diffraction (XRD, Rigaku D/max), also with electronic diffraction (Philips EM 300G), and with the help of Fourier Transform infra-red spectrometry FTIR (Nicolet 5-DX). The viscosity was measured with a BOHLIN Visco 88 BV viscometer.

3. Results and discussion

3.1. Morphological study

Particles used for the morphological investigations are directly sampled from the as-synthesized HA suspension. After dilution in ethanol, a small amount (< 1 vol %) of Darvan 7 is added to the suspension avoiding nanoparticle agglomeration.

HA nanocrystal observation with TEM shows a morphological evolution as a function of the electronic beam exposition time, energy and intensity [11]. The periphery of the particles becomes amorphous and this peripheral layer grows with the exposition time under electronic beam, Fig. 1 (a,b). HA is a very sensitive material susceptible to degrade under electronic beam. To overcome this problem the TEM investigations of HA were performed on TEM apparatus with a cryogenic stage for the sample holder.

The temperature synthesis effect on the nanoparticle shape shows that at low synthesis temperature the crystals carry a needle-shape, Fig. 2 (a). Increasing the

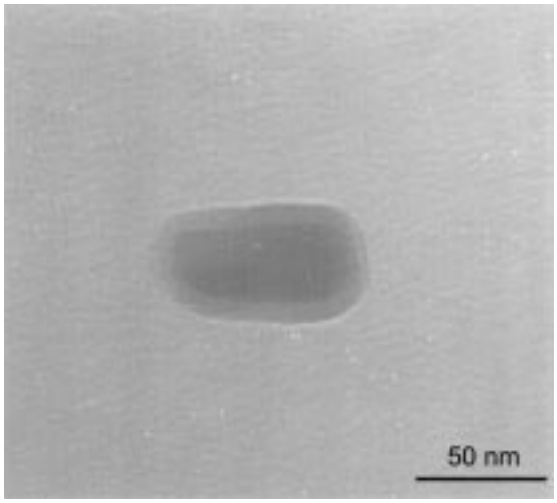

(a)

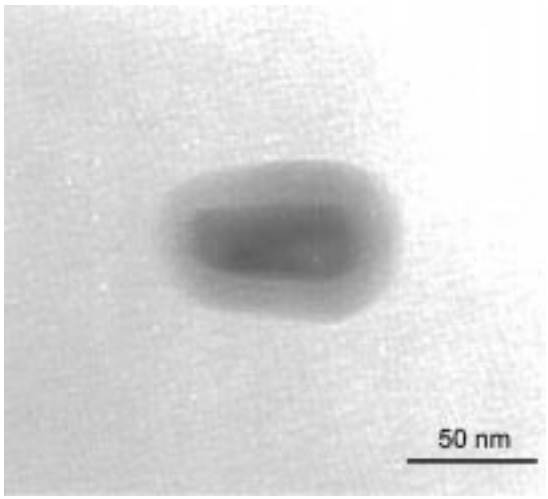

(b)

Figure 1 TEM pictures of the as-synthesized HA nanocrystals effect of electronic beam (without cryogenic stage), (a) $t = 0$; (b) $t = 3$ min.

reaction temperature changes the crystal from as-needle shape to a more regular shape close to circular, Fig. 2 (b). A shape factor can be defined by the ratio length/width of the HA nanocrystals:

$$F_s = \frac{L}{1} \tag{2}$$

where F_s, shape factor; L, particle length [m]; l, particle width [m]. The shape factor, F_s, of the HA nanocrystals decreases with an increase of the synthesis temperature. Fig. 3 shows the evolution of F_s versus the synthesis temperature.

After heating at high temperature $T = 850$ °C, 4 h, and then at $T = 1250$ °C, 4 h, the particle shape is shown in Fig. 4 (a, b) with a more regular shape in comparison with Fig. 3. Once can notice on Fig. 4a for the sample heated at 850 °C two kinds of particles:

- as-needle shaped particles such as synthesized at low temperature ($F_s = 5$)
- more homogeneous shaped particles with higher thickness ($F_s = 1.25$)

Particles of the second category are dense and result from sintering of the nanocrystals synthesized at low temperature.

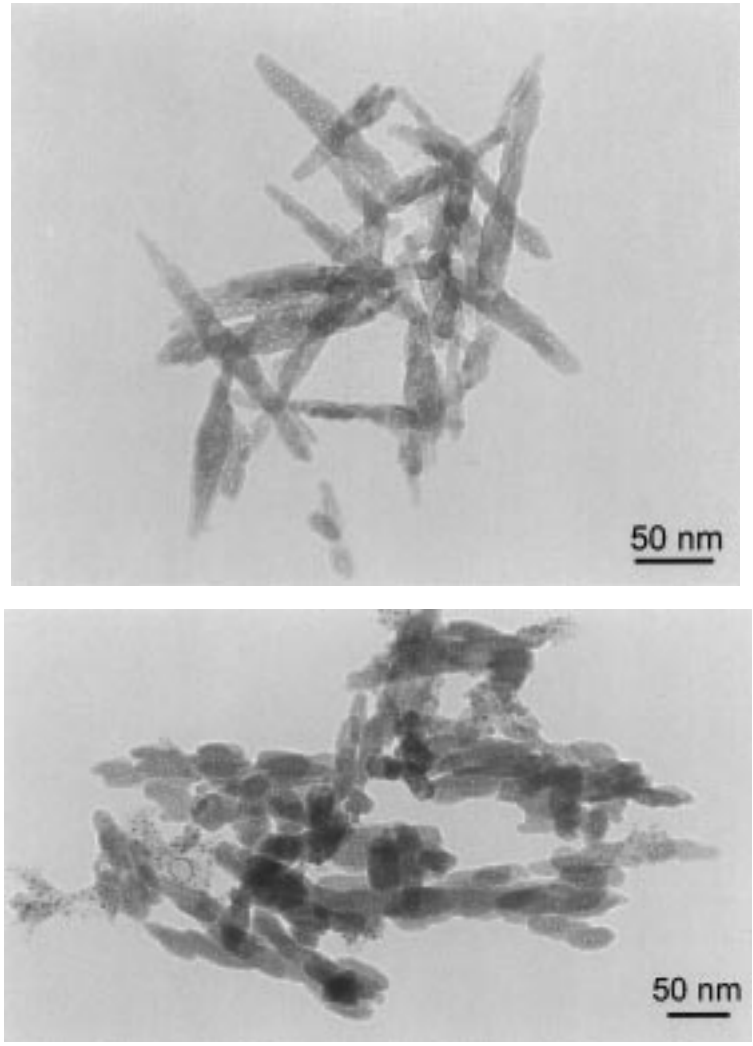

Figure 2 TEM pictures of the as-synthesized HA nanocrystals at different synthesis temperatures, (a) $T = 35\,^{\circ}\mathrm{C}$; (b) $T = 85\,^{\circ}\mathrm{C}$.

After heat treatment at 1250 °C all the particles become thicker with a shape factor close to 1, this is due to the sintering of all the particles.

Fig. 5 shows the evolution of the specific surface area (SSA) measured using the BET method, SSA decreases as synthesis temperature increases. The reaction temperature and the reactant addition rate seem to give opposite effects on the HA particle SSA, increasing the reaction temperature leads to SSA decrease while increasing the acid addition rate increases the SSA.

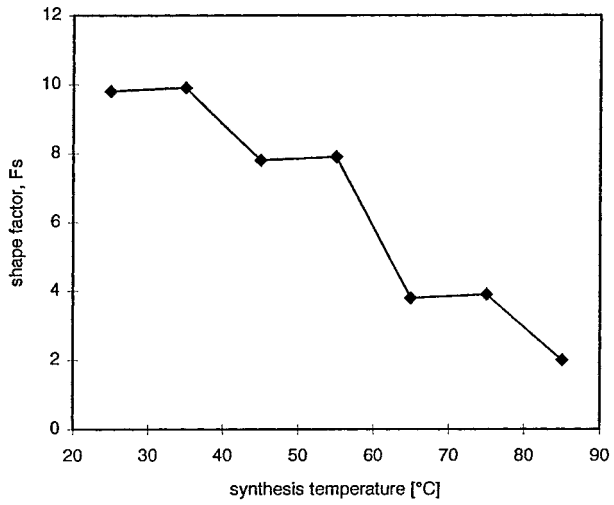

Figure 3 Evolution of the shape factor of the HA particles versus reaction temperature.

X-ray diffraction peak broadening can measure the crystallite size in a direction perpendicular to the crystallographic plane. The crystallite size $t_{(hkl)}$ perpendicular to a crystallographic family plane (hkl) can be evaluated measuring the full width at half peak maximum (FWHM) according to equation (3) expressed by the Scherrer formula [12]:

$$t_{(hkl)} = \frac{0.9\lambda}{\cos\vartheta_{(hkl)}\sqrt{\mathrm{FWHM}^2 - \mathrm{FWHM}_0^2}} \qquad (3)$$

where $t_{(hkl)}$ crystallite size [nm]; λ, wavelength of the monochromatic X-ray beam, [nm] ($\lambda_{\mathrm{K}\alpha\mathrm{Cu}} = 0$, 15418 nm); FWHM full width at half maximum for the peak sample under consideration, [rad]; FWHM_0 full width at half maximum for the peak standard under consideration, [rad]; $\theta_{(hkl)}$, exact diffraction and satisfying the Bragg's law for the (hkl) Miller's plane [°].

The peak corresponding to the (002) Miller's plane family (at $2\theta = 25.9°$) is sharper than the other peaks. This shows a trend for the crystal growth following the c-axis of the HA structure as already mentioned in [13].

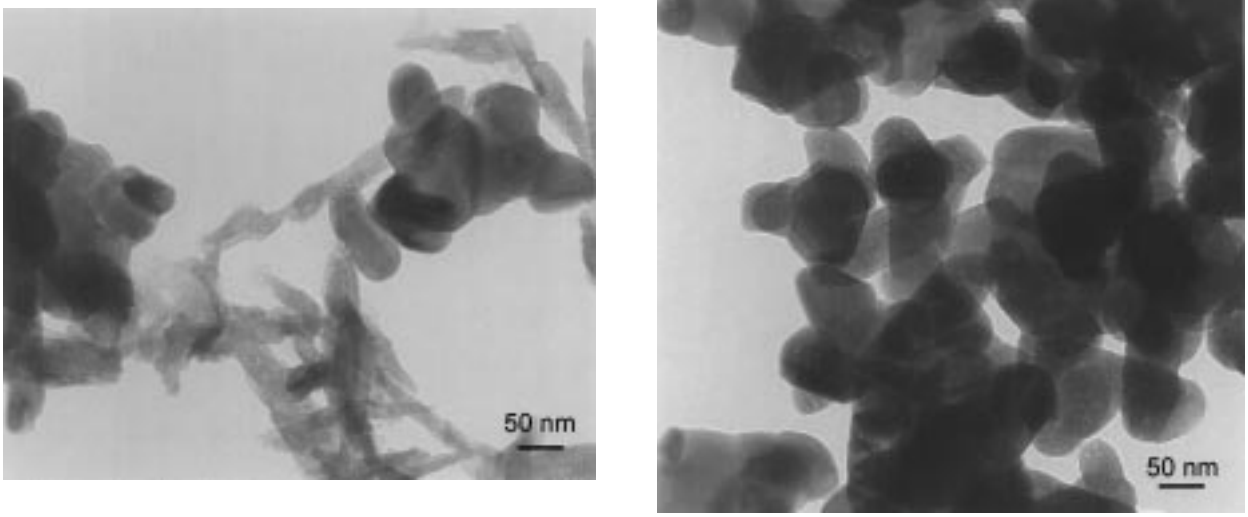

(a) (b)

Figure 4 TEM pictures of the HA particles after heat treatment at, (a) $T = 850\,^{\circ}C$, 4h (air); (b) $T = 1250\,^{\circ}C$, 4h (air).

Transmission electronic diffraction provides information at a one particle scale. The main axis of the HA particle with the needle shape corresponds to the c-axis of the HA structure. This is true for nanocrystals synthesized at low temperature ($t < 45\,^{\circ}C$), (Fig. 6a). Moreover the crystal looks like a monocrystal. At higher synthesis temperature, nanocrystals seem to loose the tendency to grow as a monocrystal following the c-axis of the apatitic structure, (Fig. 6b).

Fig. 7 shows the evolution of the crystallite size parallel with the c-axis of the HA structure. The size reaches a maximum value which corresponds to a temperature around $60\,^{\circ}C$. This phenomenon can be explained by two temperature dependent effects which are concurrent. First of all, a temperature rise increases HA crystallinity which is thermally activated. Secondly, the temperature increase limits the tendency to the monocrystalline HA nanocrystals growth following the HA c-axis, because from this critical temperature, particles become more regular and circular. Above this temperature, the tendency to grow stops. This explains the maximum size for the HA crystallites at this temperature.

In Fig. 8, $60\,^{\circ}C$ seems to be a critical temperature for the specific surface area, because at this temperature one can observe a brutal diminution of the SSA. This critical temperature can be interpreted as the limit because the speed of germination becomes higher than the speed of nucleation. In other words, above $60\,^{\circ}C$ the speed of germ creation becomes higher than their speed of growth.

The HA synthesis with quasi-instantaneous acid addition (Vadd $= 2400\,ml/min$) in the basic solution

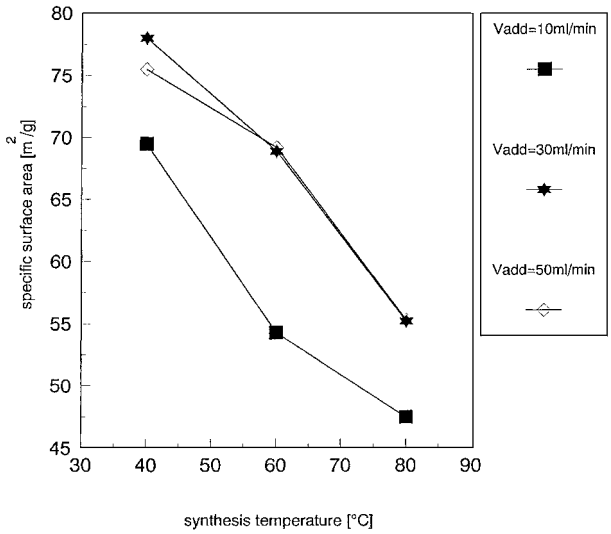

Figure 5 Specific surface area (SSA) of the as-synthesized HA nanoparticles versus reaction temperature.

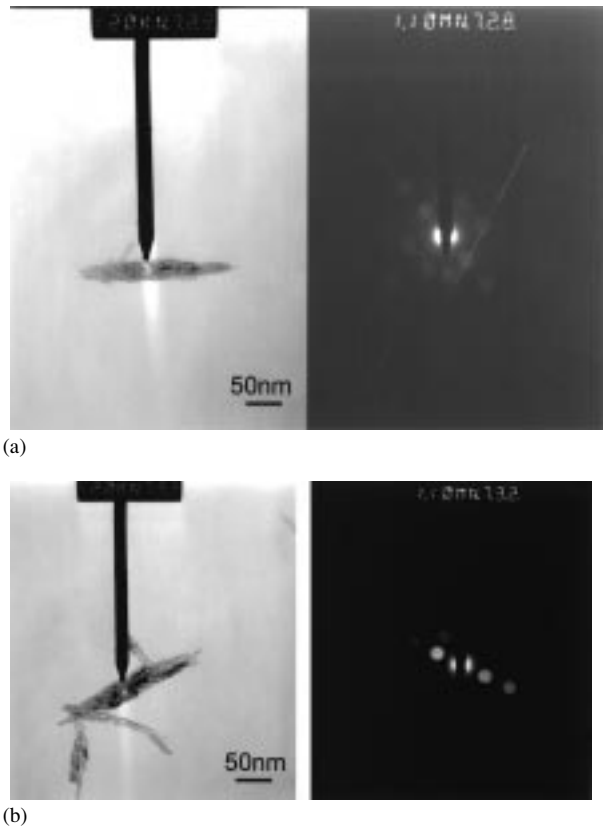

(a)

(b)

Figure 6 Electron diffraction of the as-synthesized HA particles, (a) $T = 25\,^{\circ}C$; (b) $T = 75\,^{\circ}C$.

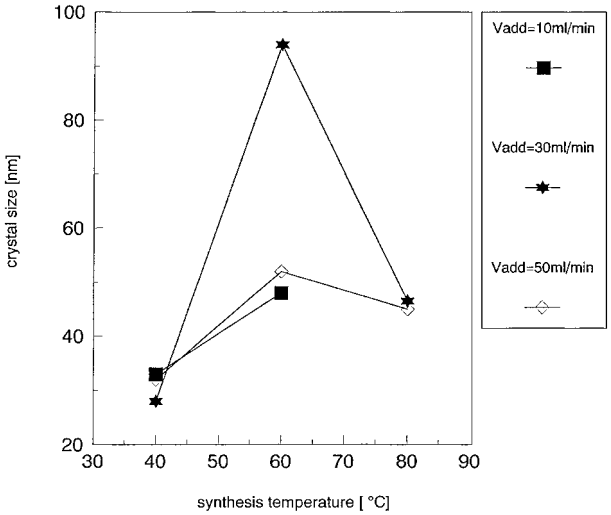

Figure 7 Crystal size following the *c*-axis of the HA nanoparticles versus the synthesis temperature.

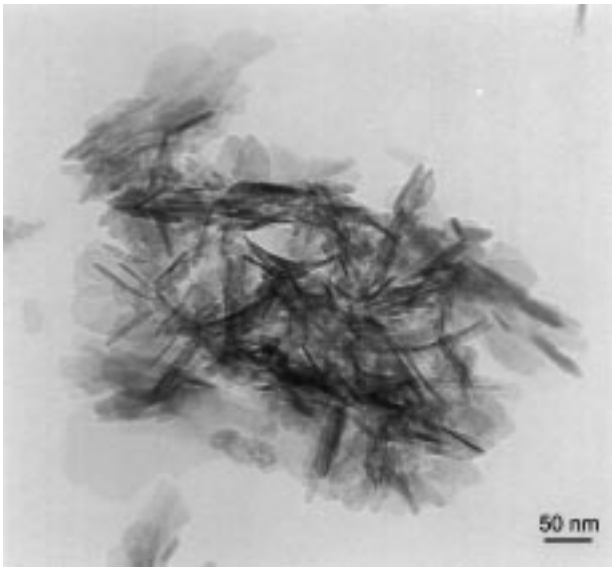

Figure 9 TEM picture of the HA nanoparticles synthesized at high acid addition rate (Vadd = 2400 ml/min).

leads to a specific morphology. Indeed, particles have an elongated shape with a very small diameter, Fig. 9. The fibrous shape gives a high shape factor ($F_s > 20$). The specific surface area reaches values higher than 90 m^2/g.

3.2. Phase composition

Phases in the precipitate are determined by X-ray diffraction (XRD). For this investigation, the water is first removed by heating at 120 °C, for 6 h. The resulting cake is crushed in a mortar. One of the problems of HA material synthesized at low temperature is the residual $Ca(OH)_2$ phase, because the more intense peak of this phase is superposed with the peak of the HA structure. Indeed, the maximum intensity peak of the calcium hydroxide which corresponds to its (101) Miller's plane is situated at 34° in 2θ scale (JCPDS#4–0733). This peak is superposed with the 25% intensity peak of HA which corresponds to the (202) Miller's plane, namely the peak situated at 34.1° in 2θ scale (JCPDS#9–432). To distinguish those phases, the sample should be submitted to a thermal heat treatment ($T = 600$ °C) which leads to the decomposition (dehydroxylation) of the calcium hydroxide to form lime with water release following the reaction:

$$Ca(OH)_2 \xrightarrow{600^\circ C} CaO + H_2O \qquad (4)$$

Lime has its 100% intensity peak, which corresponds to the (200) Miller's plane, at 37.4° in 2θ scale (JCPDS#37–1497). This peak is well isolated in this angular domain. As shown in Fig. 10(a), peaks are relatively broad, proving the poor crystallinity of the as-synthesized HA powder. In order to check the presence of calcium hydroxide in the synthesized HA, the powder is submitted to a calcination treatment at 600 °C and then to a sintering step at $T = 1250$ °C for 5 h in air. On the XRD pattern shown in Fig. 10(b) there is no parasite peak situated at 39° in 2θ scale and corresponding to the lime phase. The synthesized phase corresponds to pure HA. XRD indicates that the synthesis reaction is completed,

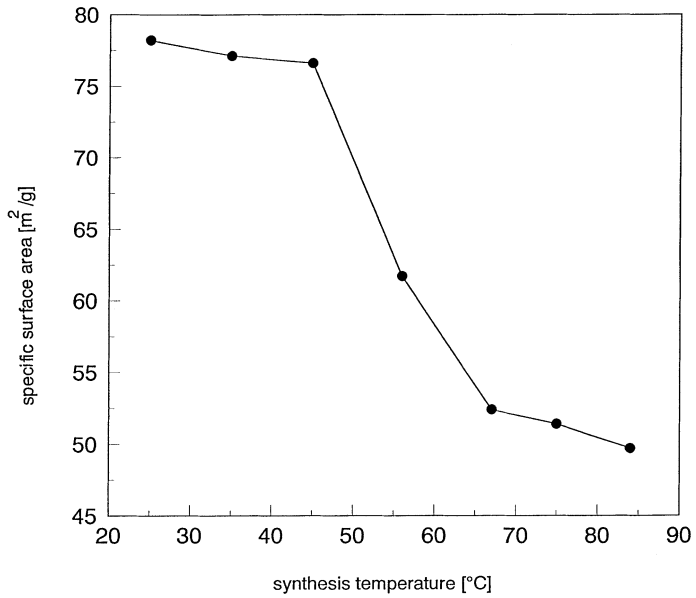

Figure 8 Specific surface area of the HA nanoparticles versus synthesis temperature.

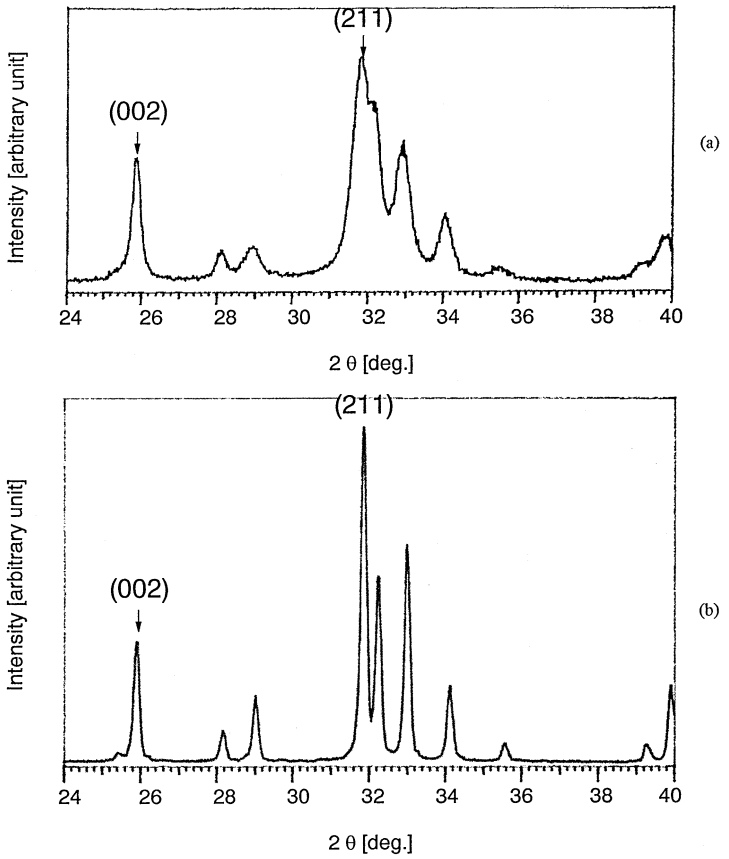

Figure 10 XRD spectra of HA nanoparticles synthesized at 45 °C and (a) heated at 120 °C; (b) heated at 120 °C calcined at 1250 °C, 5 h with air.

because there is no trace of residual reactant on the XRD spectra which indicates that reaction conversion is close to 100%. When the addition rate of the phosphoric acid is very high (Vadd = 2400 ml/ min), the synthesis reaction conversion decreases and there is some $Ca(OH)_2$ appearing in the product. When the acid addition rate is below 100 ml/min, the conversion rate of the reaction is 100%.

Infra-red spectrometry gives information concerning the molecular groups included in the unit cell of the HA structure. Fig. 11(a) shows the IR spectrum of the as-synthesized HA powders after heating at 120 °C. It indicates the presence of the OH^- groups at 3571 cm^{-1} and the triplet (564, 574 and 603 cm^{-1}) characteristic of PO_4^{3-} groups. The large peak at 3550 cm^{-1} is assigned to the crystallization water, i.e. water molecules trapped in the apatite unit cell [14]. Generally, stoichiometric HA cannot contain water molecules in its unit cell while non-stoichiometric can contain some water molecules [15].

One can notice that synthesized HA is not carbonated (no peak relative to CO_3^{2-} group), then during the synthesis there is no substitution of phosphate group by carbonate group.

The broadening of the infra-red spectrum peaks gives an indication on the crystallization state of the HA material [16]. Nevertheless, there are no direct and quantitative relationships between peak broadening and crystallite size contrary to XRD with the Scherrer formula. The observation of the infra-red spectrum of HA synthesized at $T = 45$ °C shows broad peaks, this is confirmed with the peak convolution of the phosphate triple peaks. On the contrary, the synthesized HA powder heated at 1250 °C has sharper infra-red peaks than the as-synthesized powder, Fig. 11(b). As already shown in section 3.1, the morphology of the HA particles strongly depends on the addition rate of reactant during the reaction synthesis and there is also a strong influence for the composition. A higher addition rate of acid systematically results in an increase of the $Ca(OH)_2$ content (which is not desired). This can be explained in terms of pH of the reaction media. When the acid is introduced at a very high addition rate, the pH of the reaction media decreases drastically (pH < 7). Orthophosphoric acid is a weak triacid, the acidity potentials are as follows:

$$H_3PO_4 \leftrightarrow H_2PO_4^- + H^+ \qquad pK_{a1} = 2.2 \tag{5}$$

$$H_2PO_4^- \leftrightarrow HPO_4^{2-} + H^+ \qquad pK_{a2} = 7.2 \tag{6}$$

$$HPO_4^- \leftrightarrow PO_4^{3-} + H^+ \qquad pK_{a3} = 12.3 \tag{7}$$

If $pH > pK_a$ then the dissociation of H_3PO_4 will occur according to the Le Chatelier principle. In the other case the recombination will occur. Therefore when the acid is introduced in the reaction media at a high addition rate (Vadd = 2400 ml/ min) the pH decreases leading to an incomplete dissociation of orthophosphoric acid. In the absence of PO_4^{3-}, the formation of the HA structure is compromised. This explains the presence of residual or unreacted calcium hydroxide which will further transform in lime during heat treatment. In this condition the synthesized HA can contain a fraction of dihydrogenophosphate ($H_2PO_4^-$) or hydrogenophosphate ions (HPO_4^{2-}) substituted for phosphate ions (PO_4^{3-}) which can explain the residual $Ca(OH)_2$. Even if those hydrogenophosphated phases are quite difficult to detect by XRD, their presence induces small distortions

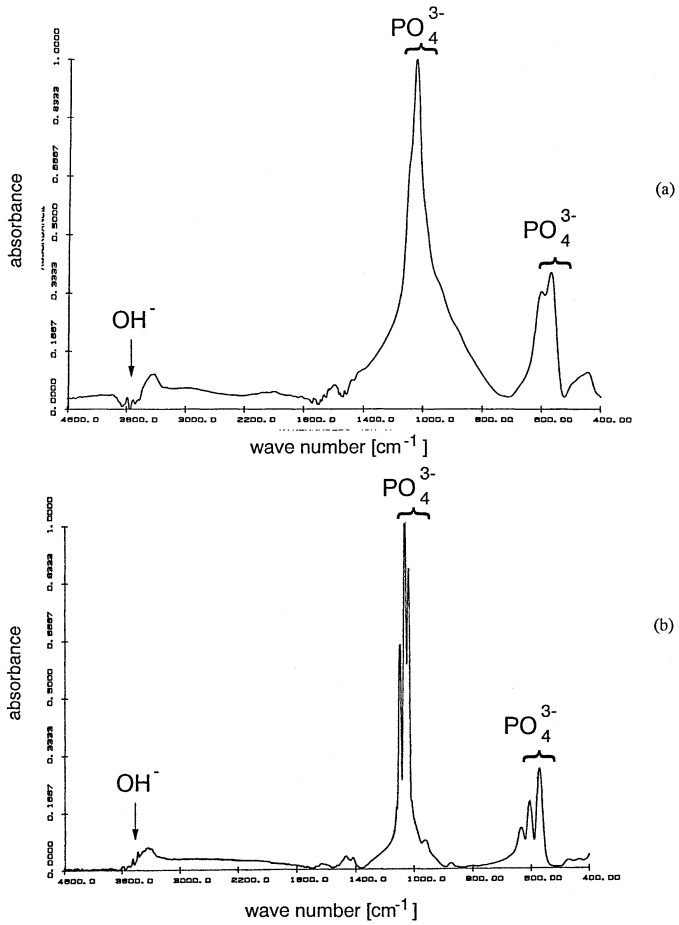

Figure 11 FTIR spectra of HA nanoparticles synthesized at 45 °C and (a) heated at 120 °C; (b) heated at 120 °C+ calcined at 1250 °C, 5 h with air.

in the unit cell. Those phases can be written in the following way: $Ca_{10-x}(HPO_4)_x(PO_4)_{6-x}(OH)_{2-x}$ with $0 < \times < 2$.

3.3. Rheological study

The requested property for HA suspension is good flowability, namely a low viscosity allowing the suspension to be pumped by a peristaltic pump.

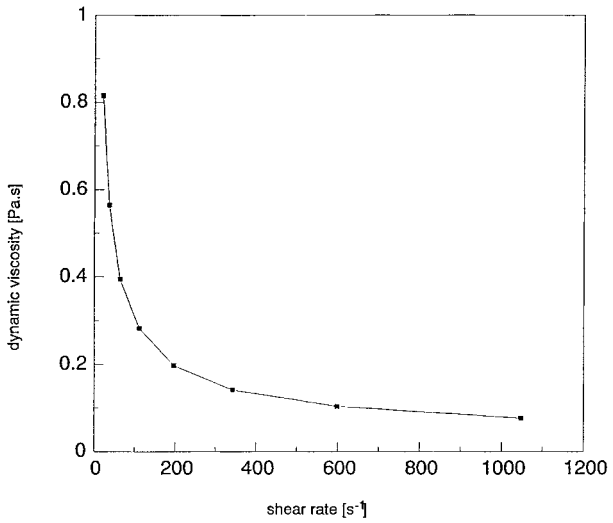

Figure 12 Viscosity of the HA suspension (40 wt % solid HA) versus shear rate (10 ml deflocculant/100 g HA).

Synthesized HA behaves as a non-Newtonian fluid, more precisely as a thixotropic fluid, Fig. 12. Elongated particles have a tendency at rest to interlace opposing any movement. Movement has to be initiated by a yield stress in order to break some link and orient the crystal. Viscosity of a thixotropic fluid decreases when shear increases. Viscosity of the as-synthesized HA suspension reach 5210 Pa with a shear rate of 1000 s^{-1}. This value is too high to permit the feeding via a peristaltic pump. To improve the flowability of the HA suspension, addition of a dispersing agent is necessary for the dispersion of HA particles in the liquid phase (water). Stability of HA depends on the zeta potential (ζ) defined by the Smoluchowski equation [17]:

$$\zeta = \frac{f_H m_e}{\varepsilon} \tag{8}$$

where ζ, zeta potential [V]; f_H, constant of Henry; m_e, electrophoretic mobility [m/s]; μ, viscosity [kg/m.s]; ε, permittivity [F/m].

The isoelectric point (IEP) is defined as the pH value associated with a ζ potential equal to zero. For HA, IEP varies between 4 and 6. For a suspension which has its pH value in this range, the stability will be poor (flocculation). In order to maintain a stable suspension, this involves a pH out of the IEP range, higher than 6 or lower than 4. For chemical stability reasons, the range of stability is chosen at higher pH values than IEP. For a moderate addition rate of acid (Vadd < 100 ml/ min) the pH at the end of the reaction is around 10. When the

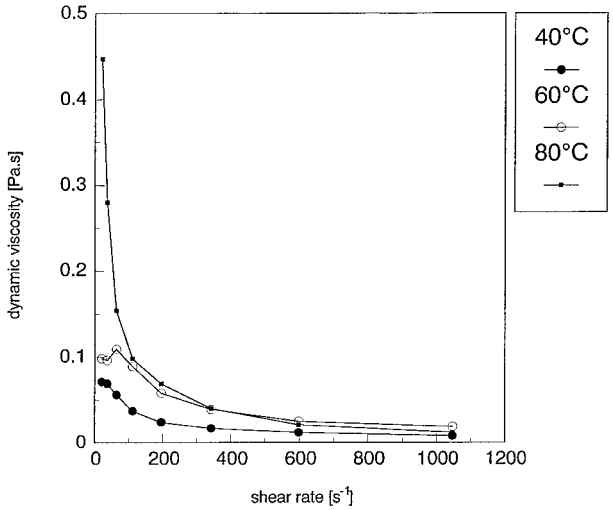

Figure 13 Viscosity of the HA suspension for different reaction temperatures (12 wt % solid HA).

addition rate of acid reaches higher values, the pH goes down close to the IEP. The natural settle time of the suspension also depends on the acid addition rate. For a high acid addition rate, the settle time is less than 5 min. Conversely, with a moderate acid addition rate, the settle time varies between 0.5 and 2 h.

The quantity of dispersing agent for the suspension suitable for atomization is 10 ml of Darvan per 100 g HA. Even with the addition of Darvan 7 the rheological behavior of the suspension is still thixotropic. Fig. 12 displays the viscosity versus the shear rate of the HA suspension suitable for atomization. The viscosity of the suspension synthesized at different temperatures is shown in Fig. 13. Viscosity seems to increase with the synthesis temperature, but the viscosity decreases with an increase of shear rate. The tendency is a diminution of the yield value and viscosity associated with a reduction of the reaction temperature. Paradoxically, the viscosity is lower when the shape factor of the particles is higher. This can be explained by the surface charge of the particle which depends on the particle specific surface area. This surface

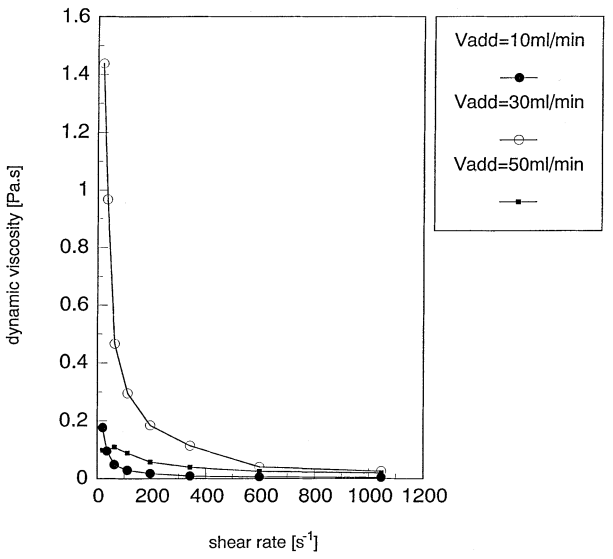

Figure 14 Viscosity of the HA suspension versus acid addition rate (12 wt % solid HA).

charge is preponderant for the stability of the suspension, therefore for good flowability and low viscosity.

In Fig. 14 the viscosity is displayed versus the shear rate for different acid addition rates. Whatever the acid addition rate, the rheological behavior is kept thixotropic. The influence of the acid addition rate is not significant. The influence of deflocculant content on suspension viscosity has been studied on suspensions with 40 wt % of HA. There is a minimum viscosity with an associated optimum deflocculant content around 10 ml/100 g HA, Fig. 15.

For the SPS application of HA suspension, which briefly allows the use of high purity suspensions or sol-gel to be atomized in a thermal plasma flame and produces either 20 μm size powder or coatings, the maximum viscosity for this process is a few Pa.s ≡ viscosity unit, above this value the suspension cannot be pumped or atomized. This is a physical limit for the use of the suspension in this process.

4. Conclusion

The chemical synthesis of HA as presented in this paper is simple to implement and the by-product (water) could be useful for the SPS process. HA synthesized particles possess a wide range of size and shape depending on the reaction temperature and also on the orthophosphoric acid addition rate. For small acid addition rates particles have an as-needle shape and for very high acid addition rates the shape factor increases until 2θ. The specific surface area of the as-needle shaped nanoparticles strongly varies with the reaction temperature, an increase of synthesis temperature limits the specific surface area to 55 m^2/g as well as the shape factor to two. One can define a transition temperature, around 60 °C, which separates domains where growing and nucleation phenomena are preponderant. Quasi-instantaneous acid addition rates (Vadd = 2400 ml/ min) lead to a different morphology of HA particles (fiber type) containing some residual and unreacted calcium hydroxide as observed by TEM. HA particle composition is mainly controled by the acid addition rate which should be maintained at a low value. The pH value at the end of the reaction, which depends on the acid addition rate, is a good indicator for the calcium hydroxide residual content. The effect of deflocculant addition to the HA suspension is a 4 order magnitude reduction of viscosity, but the rheologic behavior is still thixotropic. Finally, the favorable synthesis conditions of pure and monocrystalline HA need a moderate acid addition rate coupled with a reaction temperature lower than 60 °C, this involves a reasonably high pH at the end of the reaction (pH > 10). These conditions also satisfy other properties such as a good dispersion of the HA nanoparticles associated to an acceptable viscosity allowing the atomization of the HA suspension.

Acknowledgments

The authors would like to acknowledge the financial support of the Natural Sciences and Engineering Research Council of Canada (NSERC) and the Ministry of Education of the province of Quebec, Fond FCAR. The technical assistance of Mr P. Magny (Université de

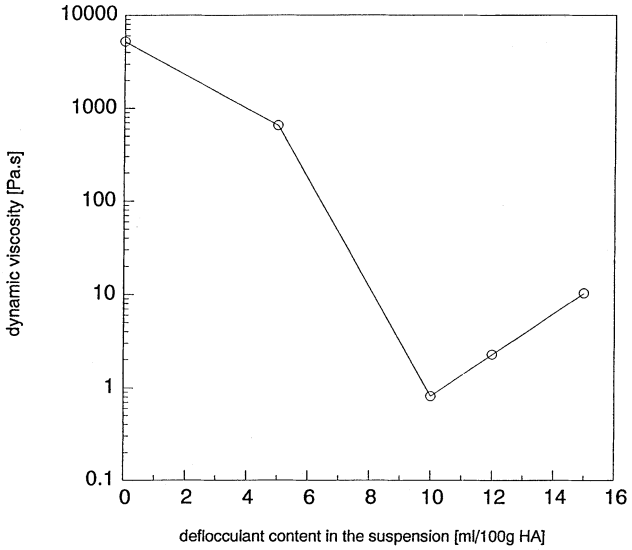

Figure 15 Viscosity of HA versus deflocculant content (40 wt % solid HA).

Sherbrooke), Dr B. Hong (CM^2, Ecole Polytechnique de Montréal) are gratefully acknowledged.

References

1. R. H. DOREMUS, *J. Mater. Sci.* **27** (1992) 285.
2. K. A. THOMAS, *Orthopedics* **17** (1994) 267.
3. Y. MASUDA, K. MATUBARAM and S. SAKKA, *J. Ceram. Soc. Jpn* **98** (1990) 1266.
4. C. CHAI, B. BEN-NISSAN, S. PYKE and L. EVANS, ''Surface Modification Technologies VII'', edited by T. S. Suddshan (Cambridge University Press, 1994) p. 509.
5. A. DEPTULA, W. LADA, T. OLCZAC, R. Z. LEGEROS and J. P. LEGEROS, in ''Bioceramics'' Vol. 9 (University Press, UK 1996) p. 313.
6. B. BEN-NISSAN, C. S. CHAI and K. A. GROSS, ''Bioceramics'' Vol. 10, edited by L. Sedel and C. Rey (Elsevier Science Ltd, UK, 1997) p. 175.
7. E. BOUYER, F. GITZHOFER and M. I. BOULOS, *JOM* **16** (1997) 57.
8. PH. COLOMBAN, *Ceram. Int.* **15** (1989) 23.
9. C. J. BRINKER and G. W. SCHERER, ''Sol-gel Science: The Physics and Chemistry of Sol-gel Processing,'' (Academic Press Inc., Boston, USA, 1990).
10. H. TAGAI and H. AOKI, ''Preparation of synthetic hydroxyapatite and sintering of apatite ceramics: Mechanical properties of biomaterials'', Chapter 39, edited by G. W. Hastings and D. F. Williams (John Wiley & Sons Ltd, 1987) p. 213.
11. J. HUAXIA and P. M. MARQUIS, *J. Mater. Sci. Lett.* **10** (1991) 132.
12. B. D. CULLITY, in ''Elements of X-ray diffraction'', 2nd edition (Addison-Wesley Publishing Company, Inc., Reading, MA, USA, 1978) p. 555.
13. L. YUBAO, C. P. A. T. KLEIN, J. DE WIJN, S. VAN DE MEER and K. DE GROOT, *J. Mater. Sci.: Mater. Med.* **5** (1994) 263.
14. K. C. BLAKESLEE and R. A. CONDRATE, *J. Am. Ceram. Soc.* **54** (1971) 559.
15. B. O. FOWLER, *Inorg. Chem.* **13** (1974) 194.
16. J. D. TERMINE and A. S. POSNER, *Nature* **211** (1966) 268.
17. J. S. REED, ''Principles of Ceramics Processing'' 2nd edition (John Wiley & Sons, Interscience, New York, USA, 1995) p. 658.

Received 21 July 1997
and accepted 8 October 1999